Nurdillayeva RN, Oshido AB, Bamford TA, El-Zubir O, Houlton A, Hedley J, Pike AR, Horrocks BR.

Inkjet printing and electrical characterisation of DNA - templated cadmium sulfide nanowires.

***Nanotechnology* 2018,**

https://doi.org/10.1088/1361-6528/aaa92f

Inkjet printing and electrical characterisation of DNA - templated cadmium sulfide nanowires

To cite this article before publication: Raushan Nurdillayeva *et al* 2018 *Nanotechnology* in press https://doi.org/10.1088/1361-6528/aaa92f

Inkjet printing and electrical characterisation of DNA - templated cadmium sulfide nanowires

R N Nurdillayeva[1,2*], A B Oshido[1], T A Bamford[3], O El-Zubir[1], A Houlton,[1] J Hedley[3], A R Pike[1] and B R Horrocks[1*]

[1] Newcastle University, School of Natural and Environmental Sciences, Chemical Nanoscience Laboratory, Bedson Building, Newcastle upon Tyne, NE1 7RU, United Kingdom

[2] Khoja Akhmet Yassawi International Kazakh-Turkish University, Natural Sciences Faculty, B.Sattarkhanov Avenue, 29, Turkistan, 161200, Kazakhstan

[3] Newcastle University, School of Engineering, Newcastle upon Tyne, NE1 7RU, United Kingdom

E-mail: raushan.nurdillayeva@ayu.edu.kz, b.r.horrocks@ncl.ac.uk

Abstract

Cadmium sulfide can be templated on λ-DNA molecules to form an aqueous dispersion of CdS/λ-DNA nanowires. Subsequent addition of ethylene glycol to 50% v/v is sufficient to formulate an ink suitable for printing using piezoelectric drop-on-demand technology. Printed droplet arrays show a coffee-ring morphology of individual deposits by fluorescence and Raman microscopy, but upon increasing the number of layers of printed material by repeated printing over each droplet, the dry deposit approaches closer to a disc shape. It is also possible to print parallel tracks by reducing the droplet separation in the array until neighbouring droplets overlap before they dry. The droplets coalesce to form a strip of width roughly equal to the diameter of the droplets. Evaporation-driven capillary flow sends the nanowires to the edges of the strip and when dry they form parallel tracks of CdS/λ-DNA nanowire bundles. Both droplets and tracks were printed onto Pt-on-glass interdigitated microelectrodes (10 μm width, 10 μm gap). The current-voltage characteristics of these two-terminal devices were approximately ohmic, but with some hysteresis. The conductance increased with temperature as a simple activated process with activation energies of 0.57 ± 0.02 eV (tracks) and 0.39 ± 0.02 eV (droplets). The impedance spectra of the printed films were consistent with hopping between CdS grains.

Supplementary material for this article is available online

Keywords: Nanowires, cadmium sulfide, inkjet printing, fluorescence, impedance

1. Introduction

DNA-templated nanowires are prepared by nucleating the growth of conductive materials (semiconductors [1-9], metals [10-19], and conductive polymers [20-25]) on DNA molecules. The role of DNA in these systems is to provide a long, thin, chemically-robust template to direct the growth of these materials as nanowires. DNA is soluble in aqueous solution and few other media; the chemistry of DNA templating is therefore dominantly aqueous and the result of these reactions is typically an aqueous suspension of nanowires. The electrical properties of DNA-templated nanowires have been characterised using the technique of molecular combing [26] to align individual nanowires across microelectrodes [2,22,27]. Conductive AFM and scanned conductance microscopy have also been employed for single nanowire electrical characterisation [19,23,24,27,28].

In general, the conductivity of DNA-templated nanowires is less than that of bulk material or other types of nanowire, e.g., VLS-grown nanowires [29]. The DNA-templated nanowires are amongst the thinnest, but their structure is often highly granular and this makes them less useful as highly conductive interconnects, but instead they have been employed as transducers in chemiresistor-type sensors [20]. Sensors employing single nanowire devices are, however, fragile: a single break disrupts the device operation completely. Instead networks of nanowires have been employed [30] because these are tolerant of breaks in single nanowires. DNA-templated nanowire networks often form spontaneously upon drop-casting of nanowire suspensions because of intermolecular interactions as the liquid evaporates. The main disadvantage of simple drop-casting is that the process is not usually well-controlled nor does it allow the formation of patterns with high resolution. Inkjet printing is potentially a superior and more controlled process, however most inks are formulated with higher concentrations of the material to be printed than is typically available for DNA-templated nanowires [31-33].

In this report we investigate the use of inkjet printing techniques to prepare defined patterns of the luminescent and semiconducting material CdS templated on lambda DNA, denoted CdS/λ-DNA. Single CdS/λ-DNA nanowires have been previously characterised by two-terminal current-voltage measurements [2]. The dual luminescence and conduction properties of CdS/λ-DNA therefore allowed us to investigate both the morphology of printed patterns by optical microscopy and the electrical behaviour of the CdS/λ-DNA when it is printed directly onto interdigitated contact electrodes. We find that the “coffee-ring” effect allows the convenient

printing of deposits of nanowires across interdigitated electrodes and improves the conductance of two-terminal devices based on DNA-templated nanowires relative to techniques based on simple drop-casting. Inkjet printing of DNA-templated nanowires is therefore shown to be a promising approach to nanowire device fabrication.

2. Experimental section

2.1 Reagents

$Cd(NO_3)_2.4H_2O$ (98%), Na_2S and ethylene glycol were obtained from Sigma Aldrich and used as received. Lambda DNA (λ-DNA, Cat. No. N3011L) was purchased from New England Biolabs UK Ltd. (Hitchin, Hertfordshire, UK). Deionised water (18 MΩ cm nominal resistivity) was obtained from a NANOpure® DIamond™ Life Science ultrapure water system equipped with a DIamond™ RO Reverse Osmosis System (Barnstead International).

2.2. Ink formulation and printing

CdS/λ-DNA nanowires were fabricated from λ-DNA and $Cd(NO_3)_2$, Na_2S by a two-stage reaction previously reported [2]. In brief, $Cd(NO_3)_2$ (200 µL, 0.2 mM) was added to λ-DNA (200 µL, 500 ng mL^{-1}) and then Na_2S (200 µL, 0.2 mM) and the reaction was incubated overnight at 4°C. Further additions of $Cd(NO_3)_2$/ Na_2S (20 µL, 20 mM) were made and the CdS/λ-DNA nanowires incubated at 4°C for 48 h. CdS/λ-DNA nanowire-containing inks were formulated by taking 500 µL of the CdS/λ-DNA solution, diluting with 500µL nanopure H_2O and then adjusting the viscosity by adding 1000 µL ethylene glycol. This gives 2000 µL of ink in which the ratio of water to ethylene glycol by volume was 1:1 (ignoring partial molar effects). Other ink formulations were also prepared for testing using different water/ethylene glycol ratios; we denote them by the percentage of ethylene glycol by volume. The ink was degassed under vacuum (20 min) prior to injection into the cartridge. Modifications to the standard printing protocols were required to use this ink with a Dimatix Materials Printer (DMP-2800). This inkjet printer has a piezoelectric head with 16 nozzles of 20 micron diameter and the nominal droplet volume is 10 pL. Using a typical platen temperature of 60°C and a 1 kHz print speed the CdS/λ-DNA nanowire inks were printed onto cleaned glass or silicon substrates, or Pt-on-glass interdigitated electrodes (Pt IDE). Dimatix Materials Cartridges (Model DMC-11610/PN 2100201146, FujiFilm, 10pL) were used in all cases. Multiple layers of the nanowires were printed to enhance the density of the final deposit. A layer corresponds

to the material deposited in one printing pass in which the print head deposits a droplet at each point of a defined array. To generate multiple layers (from 25 layers up to 250 layers, denoted 25L or 250L) of well-separated printed droplets on all three substrate types, a 100-150 micron drop spacing was used. To generate tracks of printed CdS/λ-DNA across the Pt interdigitated electrodes a reduced drop spacing of 30-40 microns was employed along with a quarter density printing technique. Details of the methodology are provided in the Supporting Information.

2.3. Preparation of substrates for printing and electrical characterisation

Glass slides were washed with water, ethanol and then sonicated in isopropyl alcohol (15 min). The slides were then oxygen plasma-cleaned (90W, 15 sccm, 10 min) and sealed overnight in the vacuum chamber of the plasma cleaner (Femto A, Diener Electronic, Ebhausen, Germany). The slides were then dried under nitrogen (30 min) directly prior to printing (60 ^{o}C). Si(111) wafers (PI-Kem Ltd., Tamworth, UK) were cut into approximately 1 x 1 cm chips, washed with acetone, dried by nitrogen, then plasma-cleaned (10 min) and dried under nitrogen (30 min) before printing.

Pt-on-glass interdigitated microelectrodes (IDEs, model IDEPt10 manufactured by DropSens) were obtained from Metrohm Ltd. (Runcorn, UK). The nominal electrode width was 10 μm and the nominal interelectrode gap was also 10 μm. However, microscopy indicated the gap to be nearer 9 μm. As-received the electrodes showed substantial background currents (nA) when a bias was applied across the contacts. These background currents were reduced to the single pA level upon cleaning. The Pt IDEs were dipped in piranha solution (conc H_2SO_4 to 30% H_2O_2 volume ratio of 1:4). They were then sonicated for 15 minutes in water, then acetone and finally ethanol. The IDEs were then dried under a stream of nitrogen, plasma-cleaned (10 min) and finally dried under nitrogen (30 min) prior to printing CdS/λ-DNA on the IDEs.

2.4 Characterisation of the printed material

The printed patterns were characterised by Atomic Force Microscopy (AFM), Fluorescence microscopy and Raman microscopy. Chemical characterisation of the ink and the printed materials employed X-ray photoelectron spectroscopy, optical absorption and infrared spectroscopy (FTIR). The chemical characterisation is available in Supporting Information.

AFM. Atomic force microscope images were acquired using a Multimode 8 AFM, a Nanoscope V controller (Bruker), an ''E'' scanner and Nanoscope software version 9.1. The system was operated in ScanAsyst-in-Air mode. An isolation table/acoustic enclosure was used to reduce vibrational/acoustic noise. Silicon tips on silicon nitride cantilevers (ScanAsyst, Bruker) were used for imaging. The nominal tip radius was about 2 nm, the resonant frequency 150 kHz and the spring constant k ~0.7 N m^{-1}. The images were analysed with NanoScope Analysis version 1.5 software (Bruker).

Fluorescence microscopy. Fluorescence images were obtained using an epifluorescence microscope (Axioskop 2, Zeiss) using AxioVision version 4.8 software (Zeiss). The excitation source was an Hg arc lamp and was bandpass filtered to give light of wavelength $300 < \lambda < 400$ nm. Back-scattered light from the sample was longpass filtered $\lambda > 420$ nm to remove elastically scattered light and the luminescence was captured on a monochrome CCD camera (AxioCam HRm, Zeiss).

Fluorescence spectroscopy. Fluorescence spectra of the CdS/λ-DNA solution were measured (Spex FluoroMax / GRAMS 32) using quartz cuvettes of 1 cm path length. The emission was detected at 90^{o} to the excitation beam and the quantum yield of the fluorescence was estimated relative to fluorescein in 0.1 M NaOH(aq) as the standard.

Photoluminescence dynamics. PL lifetimes of the CdS/λ-DNA solution were measured using an Edinburgh FLS980 photoluminescence spectrometer, equipped with Czerny Turner excitation and emission monochromators (1.8 nm/mm dispersion; 1800 grooves/mm), a time-correlated single photon counting (TCSPC) module and a Hamamatsu R928P photomultiplier tube (in a fan-assisted TE cooled housing, operating temperature -20 °C). For lifetime measurements, samples were excited with an EPL-475 (471.8 nm; 61.1 ps pulse width) picosecond pulsed diode laser.

Raman microspectroscopy. A confocal microscope (WiTec Confocal Raman Microscope model CRM200, Ulm, Germany) was used to record Raman images and spectra of the printed samples. A diode laser of 60 mW output power at a wavelength of 488 nm was used as the excitation source. Emitted light was transmitted through a Raman edge filter to attenuate the elastically scattered component and collected by a multimode optical fiber which also served

as the confocal pinhole. The light was then dispersed on a grating (150 lines mm^{-1} or 1800 lines mm^{-1}) and detected using a Peltier-cooled CCD (-60ºC).

X-ray photoelectron spectroscopy, XPS. A Kratos Axis Ultra 165 photoelectron spectrometer equipped with a monochromatic Al Kα X-ray excitation source (1486.7 eV) was used to collect photoemission spectra (NEXUS, Newcastle University). The operating power was 150 W (15 kV, 10 mA) and the chamber pressure was ~3×10^{-9} Torr. The photoelectrons were filtered by a hemispherical analyzer and recorded by multichannel detectors. Spectra were recorded with a step size of 0.1 eV. The binding energies obtained in the XPS analysis were calibrated using the lowest C1s component (284.6eV) as a reference. Spectral peaks were fitted using the CasaXPS software version 2.3.16 from Casa Software Ltd. (Teignmouth, UK). Samples were prepared by drop-casting ~20 μL CdS/λ-DNA onto clean Si chips.

Optical spectroscopy. UV-Vis spectra of aqueous dispersions of CdS/λ-DNA were recorded on a NanoDrop One absorption spectrometer (ThermoFisher Scientific). Sample volumes of 1.5 μL were used and water was the background. The absorbance values reported have been scaled to a standard pathlength of 1 cm by the instrument software.

Infrared spectroscopy. FTIR spectra were recorded using the ATR accessory of an IRAffinity-1S Fourier transform infrared spectrophotometer (Shimadzu) operating with 4 cm^{-1} spectral resolution and equipped with a DLATGS detector. The sample was drop-cast as a dry film on a Si(111) chip and a clean Si(111) chip was used as a background. 32 spectra were co-added and averaged.

2.5 Electrical characterisation.

CdS/λ-DNA was printed onto the Pt-on-glass IDEs either as an array of droplets or as a set of parallel tracks. The IDEs were maintained at 60ºC during printing to facilitate drying of the ink. Conductivity measurements at controlled temperature (I-V-T measurements) were performed on a Cascade Microtech probe station using an Agilent B1500A parameter analyser. The sample chamber was maintained under a dry nitrogen atmosphere in the absence of illumination and the temperature was controlled by a thermal chuck system (Model ETC-200L, ESPEC, Japan). Impedance spectra were recorded at zero dc bias using an Ivium

CompactStat(e) potentiostat (Alvatek, UK Ltd) with an ac amplitude of 0.1 V and 10 frequencies per decade over the range 10^4 – 10^{-1} Hz.

3. Results and discussion

The results and discussion are organised in 3 sections: ink formulation; characterisation of printed CdS/λ-DNA nanowires and electrical characterisation of the printed inks. Chemical characterisation of the CdS/λ-DNA is available in the Supporting Information. The effect of additives (ethylene glycol) necessary for ink formulation on the nanowires is briefly investigated by AFM. The morphology and composition of printed droplets and tracks is studied by fluorescence, AFM and Raman microscopy. Finally the electrical properties of CdS/λ-DNA droplets and tracks printed on interdigitated electrodes are compared using two-terminal I-V measurements and impedance spectroscopy. The overall procedure is illustrated schematically in scheme 1.

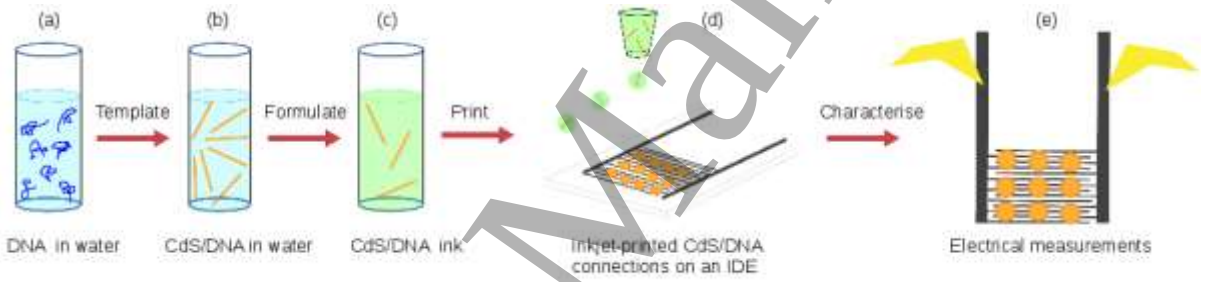

Scheme 1. Schematic of the process for testing CdS/λ-DNA inks. From left to right: (a) λ-DNA dispersed in aqueous solution; (b) a dispersion of CdS/λ-DNA nanowires; (c) the CdS/λ-DNA ink after addition of ethylene glycol to modify the viscosity; (d) an array of printed CdS/λ-DNA dots on a Pt-on-glass interdigitated electrodes (IDE). The Pt line width is 10 μm and the interelectrode gap is ~9 μm and (e) electrical characterisation of the printed array using a probe-station or potentiostat to contact the IDE.

3.1 *Formulation of CdS/λ-DNA nanowire inks*

The typical inks employed in materials printing are more concentrated than the dilute aqueous solutions of DNA employed in templating nanowires [32,33]. The use of dilute aqueous solutions in inkjet printing presents issues because of the amount of material deposited in each droplet, droplet spreading and the rheological properties of the ink [34]. In order to print in a controllable manner on the hard, non-absorbent substrates required for the electrical characterisation, we investigated the use of ethylene glycol in the ink formulation, multi-pass printing protocols and temperature control of the substrate. The rheological properties of inks are well-known to be crucial for the printing process [34]. Ethylene glycol is a standard additive

used in aqueous ink formulation and therefore we considered the effect of its addition on the properties of the CdS/λ-DNA nanowire suspensions. After formation of the CdS/λ-DNA nanowires, varying concentrations of ethylene glycol were added to the nanowire suspension and the morphology of the subsequent drop-cast (figure 1) and printed (figure 2) nanowire deposits were examined by AFM.

Figure 1 shows individual CdS/λ-DNA nanowires imaged after drop-casting 10 μL of CdS/λ-DNA ink with varying amounts of ethylene glycol. The cast drops were left on the Si chip for 15 minutes and then blown dry with a stream of dry nitrogen. This procedure has the effect of combing the nanowires in the same manner as bare DNA molecules [26]. Variation of the ethylene glycol content from 0% to 75% (v/v) on the conformation of the nanowires was investigated by AFM after drop-casting the ink on silicon wafers. Figures 1a-d show two effects of ethylene glycol: (i) the bundling of multiple strands to form "ropes" is less evident in the presence of ethylene glycol, however (ii) at high ethylene glycol concentration (figure 1d), few extended nanowires are observed. Section analysis of the individual strands indicates a typical height of 3 – 5 nm corresponding to CdS-coated rather than bare DNA (1-2 nm).

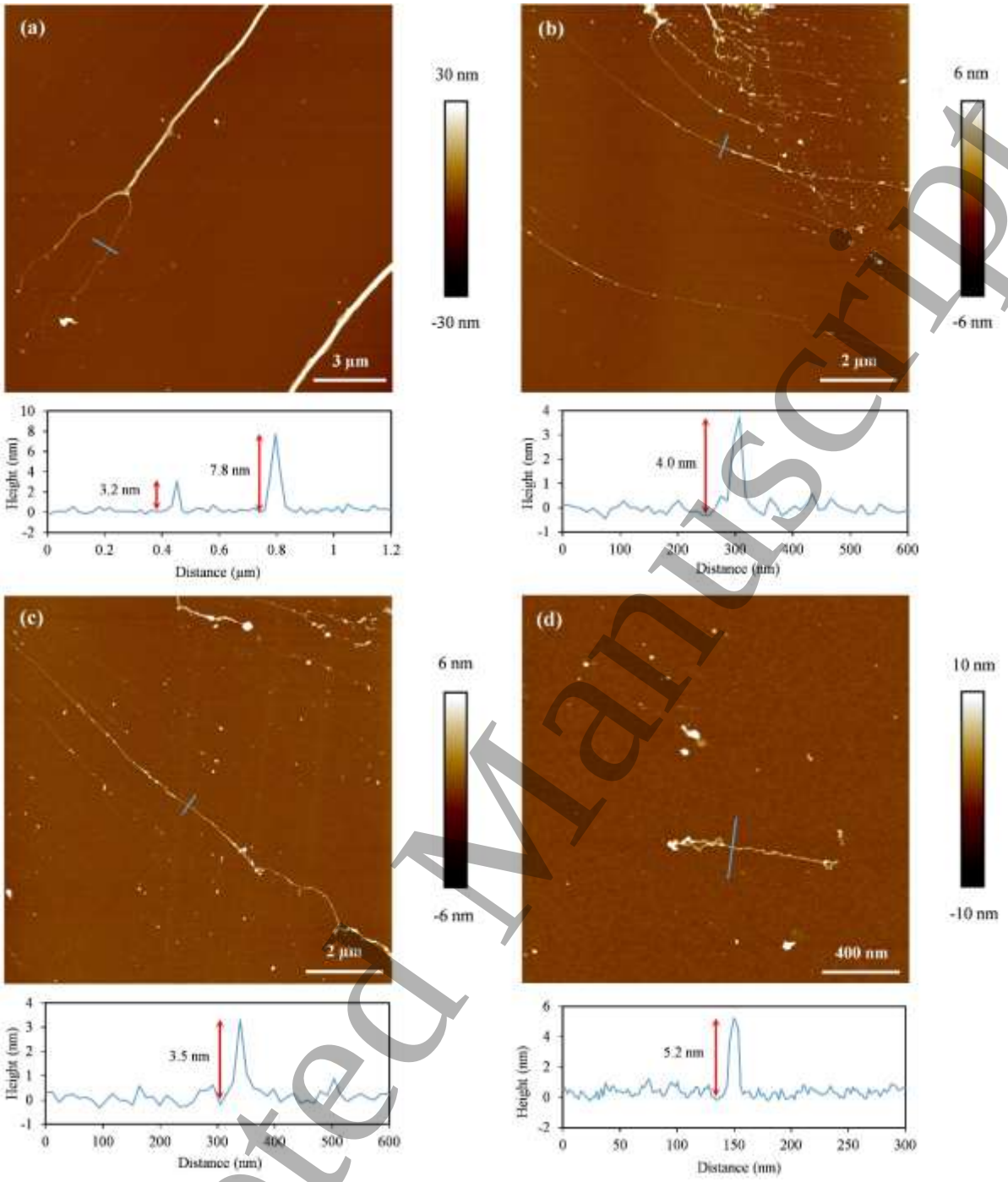

Figure 1. AFM images of drop-cast CdS/λ-DNA inks of varying ethylene glycol volume fraction. In all cases the substrate was an Si(111) chip. **(a)** 0%; **(b)** 25%; **(c)** 50% and **(d)** 75% ethylene glycol. The section profiles below each image show the heights of typical nanowires.

CdS/λ-DNA nanowires maintain an extended conformation when cast from aqueous solutions and also in the presence of ethylene glycol up to about 50% v/v. However, too high a volume fraction of ethylene glycol (75%) was found to result in coiling/compaction of the CdS/λ-DNA. Even though we are not aiming to construct single-nanowire devices, nevertheless it is desirable for the nanowires to retain a more or less extended conformation because previous

observations indicate that the length of the nanowires affects the conductance even in films of nanowires [35]. Coiled or compact deposits of nanowires are more likely to produce breaks in the conduction pathway through a deposited film. The chemical reason for this compaction is likely to be simply that ethylene glycol is a poor solvent for DNA: water is a superior hydrogen-bond donor and possesses a higher relative permittivity [36,37].

Dilute aqueous inks combine low viscosity and high surface tension; these factors result in poor droplet generation and instability and lead to poor printing resolution. Addition of ethylene glycol increases the ink viscosity and gives rise to more nearly spherical and more stable droplets. In addition, the tendency of the droplets to spread on the substrate before evaporation and deposition of the nanowires is reduced; these factors improve pattern resolution. The highest fraction of ethylene glycol compatible with the extended nanowire conformation is therefore optimal. For these reasons, we employed the 50% ethylene glycol ink throughout the rest of the work for printing CdS/λ-DNA nanowires.

Figure 2a shows an AFM image of a small part of a 50% ink CdS/λ-DNA nanowire deposit printed onto an Si chip. The image illustrates the network of nanowires formed as the aqueous dispersion of nanowires dries; the nanowires are visible in the image as long, entangled fibres. The small bright spots are salt crystals originating from the buffer in which the DNA is supplied. Such networks are crucial for the construction of useful electrical sensors because compacted or aggregated nanowires would not form effective conduction pathways across an interelectrode gap of the order of 10 micrometres.

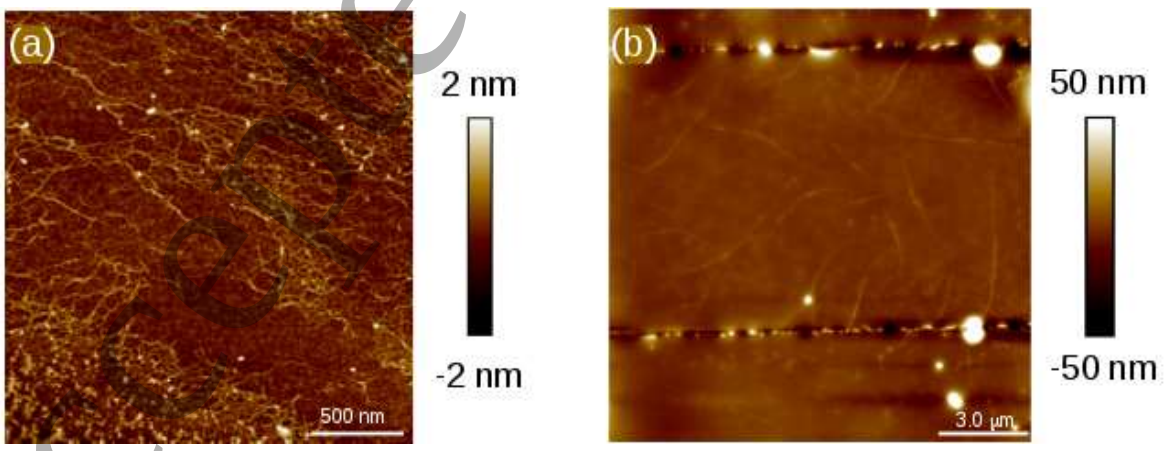

Figure 2. AFM images of **(a)** CdS/λ-DNA nanowires; 100 layers (100L) printed as a droplet on a Si chip (scale bar 500 nm) and **(b)** CdS/λ-DNA nanowires; 50L printed as a track on Pt interdigitated microelectrodes (scale bar 3 μm).

Figure 2b is an AFM image of some CdS/λ-DNA nanowires printed onto Pt-on-glass interdigitated electrodes. The boundary between the Pt electrodes and the glass is observed as lines running approximately east-west near the top and the bottom of the image where the rough edge of the Pt shows as bright spots. The area between the lines is the bare glass interelectrode gap, which is covered with CdS/λ-DNA nanowires. The area imaged is at the edge of a printed deposit in order to allow visualisation of individual nanowires; near the centre of the deposit, the film is too thick to resolve individual nanowires by AFM and was studied instead by fluorescence microscopy below (figures 4, 5). The image of figure 2b shows parts of the nanowires as randomly arranged fibres. We cannot resolve the full length of each fibre because the roughness of the substrate obscures the relevant details. However, the electrical measurements below do confirm that they span the gap. The data in figure 2 demonstrates that it is feasible to print CdS/λ-DNA nanowires, whilst retaining their extended conformation and to print deposits across contact electrodes. More detailed characteristaion of the printed droplets required also fluorescence and Raman imaging as well as AFM.

3.2 *Morphology of printed CdS/λ-DNA nanowire deposits*

DNA-templated nanowires prepared from λ-DNA are necessarily dilute because (i) the available commercial preparations of λ-DNA have concentrations of order 500 ng mL^{-1} and (ii) use of too high a material : template ratio results in the formation of particles rather than nanowires [38]. Inks comprising various metallic nanomaterials [39-43] are typically prepared at high concentration because the aim is to print conductive electronics or transparent conductive layers where low sheet resistance is important. Binary semiconductors such as CdS are of interest for different reasons and in applications where high conductivity is less important, e.g., as fluorescent labels and as chemically-sensitive transducers for sensing [44,45]. Nevertheless, it is necessary to print multiple layers of CdS/λ-DNA nanowires in order to build up a thickness suitable for fluorescence microscopy or electrical sensing devices. This can be simply achieved by printing droplets in a pre-defined array and then returning to the initial point and printing over the array again. In this context, a layer means a single printing pass and the thickness of the printed deposit depends on the ink concentration and the number of layers (L). As long as the ink dries before the print head returns for another pass, the thickness of the printed deposits can be controlled by increasing the number of layers.

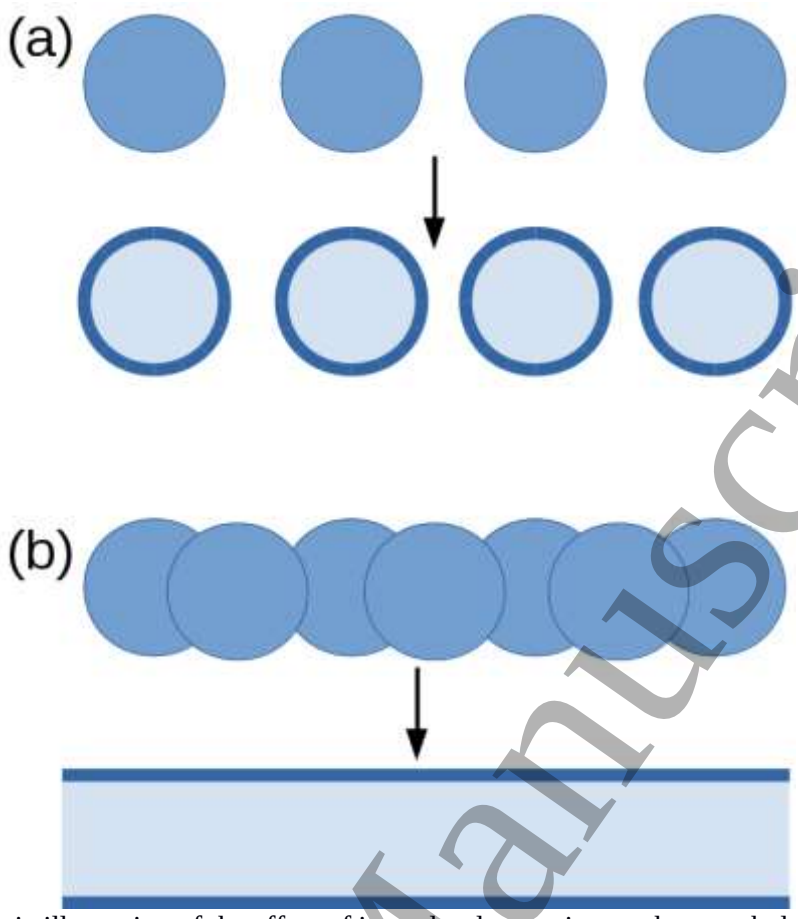

Figure 3. Schematic illustration of the effect of inter-droplet spacing on the morphology of the printed deposit after drying (black arrows). **(a)** Well-separated droplets give rise to a 'coffee-ring' morphology because of capillary flow effects [46] and **(b)** closely-spaced droplets dry to produce parallel tracks of material. The dark blue lines in the scheme indicate the concentration of printed nanowires at the droplet perimeter or the edge of a strip formed by overlapping droplets.

As well as the number of layers, the inter-droplet spacing is important (detailed printing protocols are given in supporting information). We demonstrate two limiting cases, the first where the droplets are sufficiently far apart (100-150 μm) that they do not overlap before they dry and the second where the droplets are deliberately printed close together (30-40 μm) so that they overlap. In the first case, the final observed pattern is simply an array of CdS/λ-DNA spots whose morphology and thickness is examined in figures 4 - 7. In the second case, the droplets overlap to form a wetted strip and subsequently dry as two parallel tracks, whose separation is determined by the droplet diameter on the substrate. This is useful for printing across electrical contacts, e.g., interdigitated electrodes and is examined in figure 8 below.

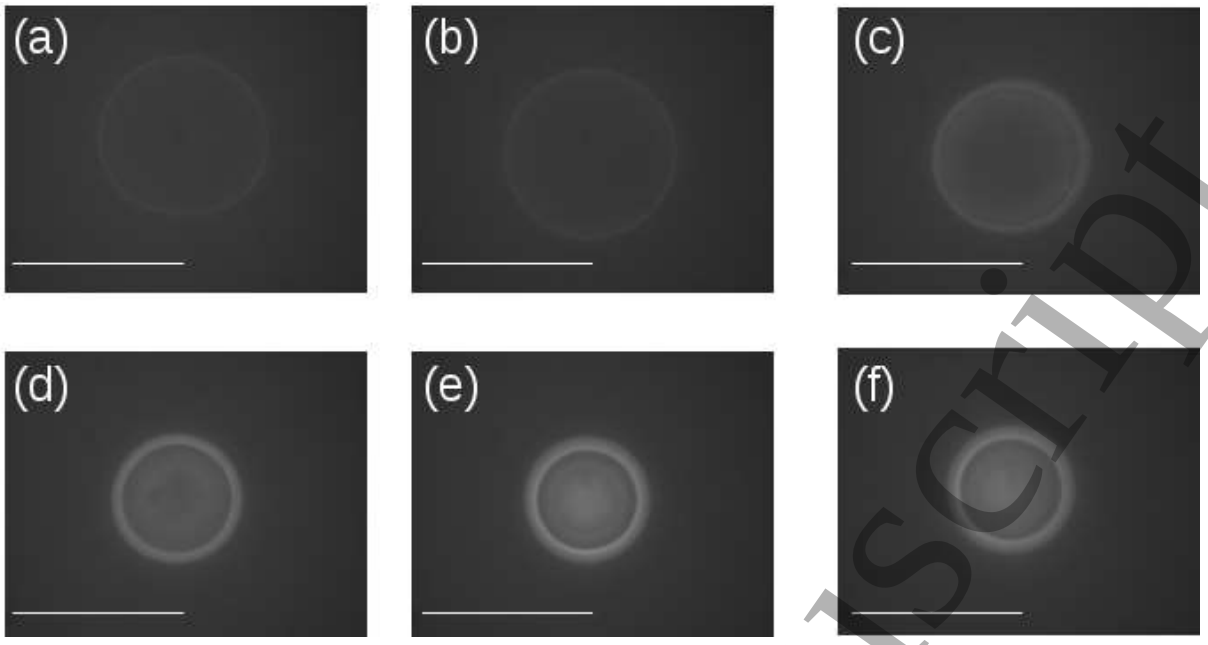

Figure 4. Fluorescence images ($300 < \lambda_{exc} < 400$ nm, Hg lamp, $\lambda_{em} > 420$ nm) of CdS/λ-DNA+50%Ethylene Glycol printed as droplets with different numbers of layers (L) at 60^0C on a glass substrate: **(a)** 25L, **(b)** 50L, **(c)** 100L, **(d)** 150L, **(e)** 200L, **(f)** 250L (scale bar = 100 μm).

Figure 4 shows a series of images of individual printed droplets of CdS/λ-DNA nanowires. All the droplets are printed under identical conditions, except with increasing number of print layers from 25L (figure 4a) to 250L (figure 4f). Each droplet is one example from an array of droplets. First, the print head deposits a drop of ink at each point in the array in turn; at this time each point in the array is one "layer" deep. The print head then returns to the first point in the array and deposits another drop on top of the original and proceeds through the array in the same manner, after this process each droplet is now two layers thick. The aim of the experiment was to observe the changes in the morphology of the final, dried, printed droplet as a function of the number of layers. Figure 4a shows a 25L droplet, which fluoresces under UV (λ = 300-400 nm) excitation because of the emission from CdS; DNA does not luminesce nor indeed absorb light at these wavelengths. It is clear that the size and the structure of the printed droplet changes with layer number. At layer numbers $L < 100$ a clear "coffee ring" morphology is observed [46]; evaporative flows well known in inkjet printing drive the dispersed material to the edge of the drying droplet. However, for layer numbers $L > 150$, the ring changes towards a disc morphology. Two factors are likely to contribute to the change of morphology: (i) the droplet contact line is pinned at smaller radii when there is a ring of solid material present instead of a clean surface and (ii) Marangoni effects are known to oppose the coffee-ring effect [47]. Evidence for the former can be seen in the appearance of concentric rings in, e.g., figures 4c-f. However it is also known that nanofibres [48] are particularly effective at suppressing the

coffee-ring effect and it seems likely that the increase in surface concentration of CdS/λ-DNA nanowires with layer number would have a similar result. The apparent droplet size also decreases, which suggests the new material is dominantly concentrated in the centre of the ring at higher layer numbers. Nevertheless, it is clear that some control of the morphology of the printed material is possible: in cases where transparency of the printed image is useful, it may be preferable for the coffee-ring morphology to be achieved and this is possible simply by controlling the printing protocol.

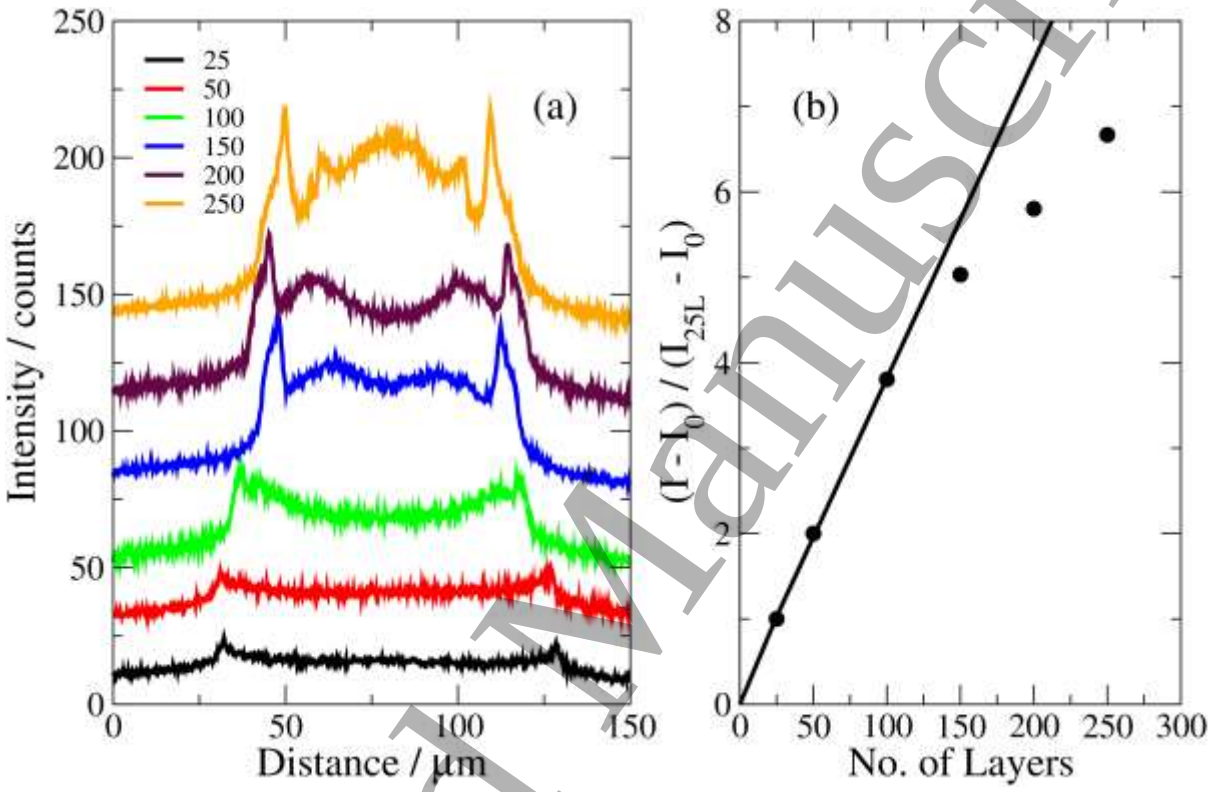

Figure 5. (a) Intensity against distance across the diameter of the droplets in figure 4 and **(b)** integrated intensity (I) over each droplet against the number of layers (25L, 50L, 100L, 150L, 200L, and 250L). The droplets were printed on glass substrates at 60^0C from 50% ethylene glycol ink containing CdS/λ-DNA nanowires. The spectra in (a) have been offset for clarity. The integrated intensities in (b) have been corrected for the background (I_0) and normalised to the intensity of the 25L sample (I_{25L}).

Figure 5 shows in greater detail the effects observed qualitatively in figure 4. Figure 5a (black) is a cross-section through the fluorescence image of the 25 layer droplet of figure 4a and figure 5a (orange) is a similar cross-section through the image of the 250 layer droplet of figure 4f. The curves between 5a (black) and 5a (orange) correspond to 4b-e. These profiles show clearly the ring morphology for layers 25-100 and the addition of material to the centre for L > 150. It is also clear that the overall intensity of each profile increases with layer number – the additional material for layers > 150 is not solely added to the centre, but the ring at the droplet edge also increases in intensity.

In order to quantify the data of figure 5a, we integrated the fluorescence signal over a square region of the image (of constant size) and evaluated the mean fluorescence intensity. After subtraction of the background (I_0) and normalization of the results to the value for the 25 layer droplet (I_{25L}), the data is plotted in figure 5b. It is clear that there is a proportionality between layer number and intensity up to nearly 150 layers. This is consistent with expectations based on no loss of CdS material with increasing layer number. Above 150 layers, the plot is sublinear. This cannot be explained on the basis of the change in droplet radius because the evaluation of the mean intensity accounts for all the fluorescence of each printed droplet. However, sublinearity in this kind of fluorescence data is not wholly unexpected because sufficiently thick layers will be subject to inner filter effects: when the absorption depth of the excitation light is less than the layer thickness not all the material deposited will be excited. In addition, self-quenching effects or self-absorption may become important.

The topography of the printed droplets and tracks was also characterised by atomic force microscopy (AFM) in figure 6. The change in droplet morphology with increasing number of printed layers that was observed by epifluorescence microscopy (figure 4) is also observed by AFM. The droplet edge region – the characteristic coffee-ring - becomes thicker with layer number, but the width also increases.

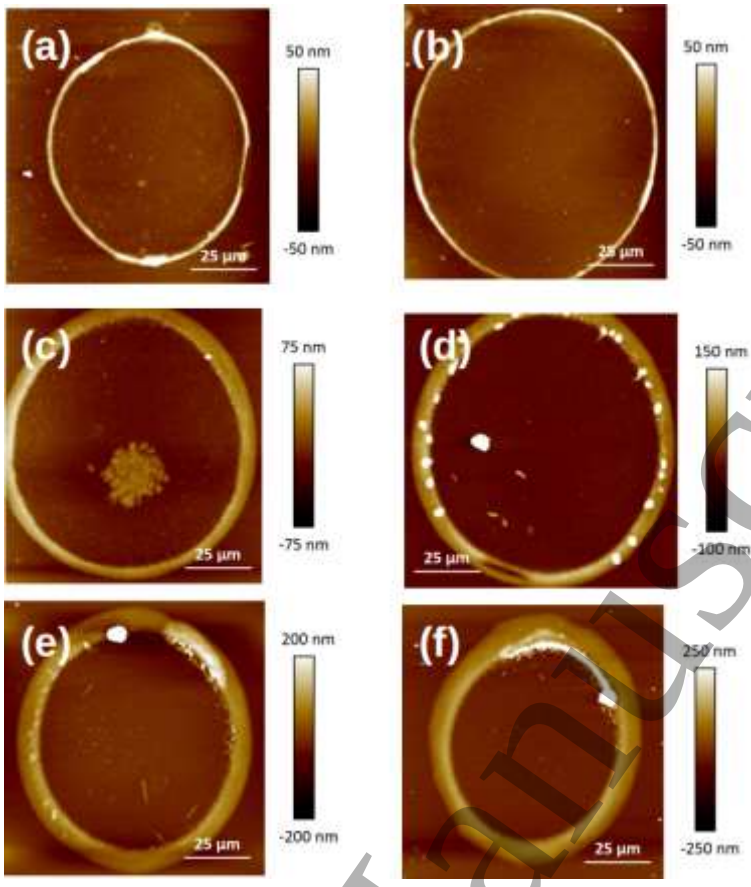

Figure 6. AFM images of printed CdS/λ-DNA droplets printed with different numbers of layers, L. **(a)** L=25; **(b)** L=50; **(c)** L=100; **(d)** L=150; **(e)** L=200 and **(f)** L=250.

More details of the printed droplets are shown in figure 7. The section profile over the edge region of several printed droplets (figure 7a) shows the increase in the thickness of the printed deposit and the increase in the width of the edge region

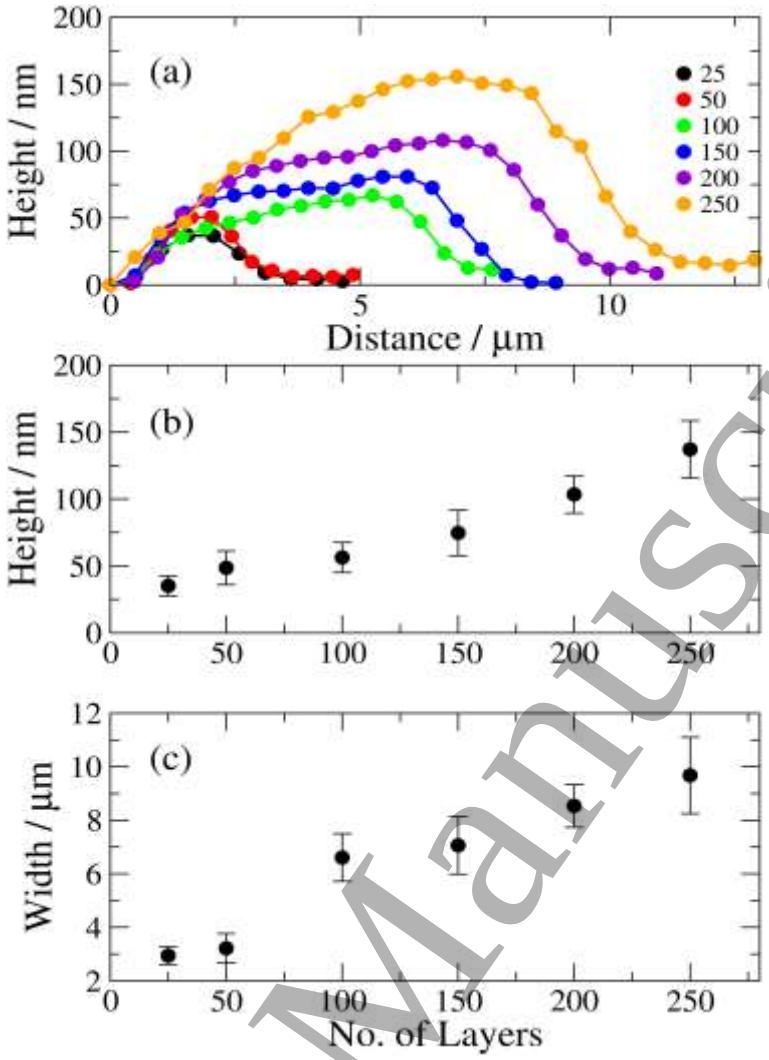

Figure 7. (a) AFM height profiles across the edge region of printed droplets. The legend indicates the no. of printed layers, L. **(b)** Maximum height of droplet edge regions against layer number, L. The values plotted are the means and sample standard deviations determined from 20 AFM height profiles. **(c)** Width of the edge of printed droplets against layer number, L.

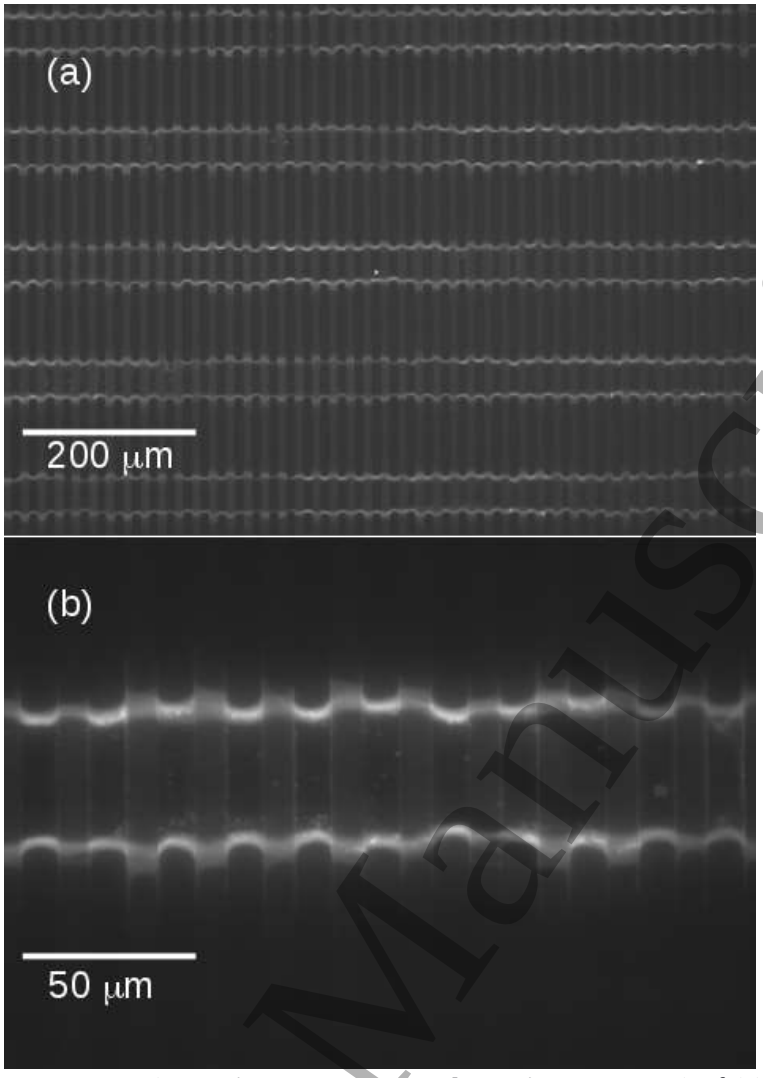

Figure 8. Fluorescence images ($300 < \lambda_{exc} < 400$ nm, Hg lamp, $\lambda_{em} > 420$ nm) of **(a)** 50% CdS/λ-DNA nanowires printed as a track 50L on Pt-on-glass IDEs. **(b)** at higher resolution.

As well as printing droplets, we have also found that it is possible to print tracks of CdS/λ-DNA nanowires. This protocol takes advantage of the coffee-ring effect. By printing a linear array of droplets sufficiently close together that they overlap before they dry, the droplets coalesce to form a continuous wet strip. The nanowires are driven to the edge of the strip by capillary flow during evaporation of the solvent and therefore, when dry, the printed image has the form of a train track with two parallel rails (figure 3b). Importantly, a quarter density printing approach was required to form these features. This technique involves printing each layer of material in separate lower-density print cycles, in order to prevent uncontrolled wetting of neighbouring ink droplets (Supporting Information). Figure 8 shows an example in which the tracks are printed across a Pt-on-glass interdigitated electrode. In figure 8a 5 rows of droplets (5 tracks each with 2 rails) are visible running east-west across the image. Figure 8b shows a higher magnification fluorescence image of a single track. The rails are not perfectly

straight on the IDE because of the change in surface properties at the Pt/glass boundary. The tracks in figure 8 were printed so that they lie across the Pt electrodes (visible as brighter strips running north-south and interdigitated with bare glass). This orientation is desirable for electrical characterisation so that the network of CdS/λ-DNA nanowires spans the gaps between the Pt microelectrodes.

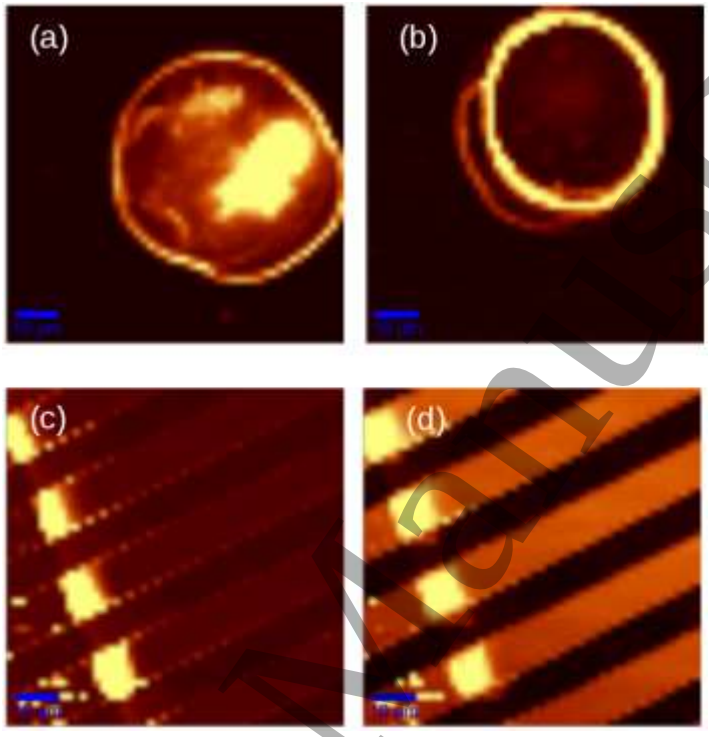

Figure 9. Raman images. **(a,b)** CdS/λ-DNA 50% nanowires printed as separate droplets on glass. The images comprise 50 x 50 pixels and the spectrum at each pixel was obtained by dispersing the back-scattered light on a coarse grating (150 lines mm^{-1}). **(a)** Printed on a glass substrate at 100ºC, 100L; **(b)** Printed on a glass substrate at 60ºC, 100L. **(c,d)** CdS/λ-DNA nanowires printed (60ºC, 50L) as tracks across a Pt-on-glass IDE. The images comprised 50 x 50 pixels and the gratings used were (c) 1500 lines mm^{-1} and (d) 1800 lines mm^{-1}.

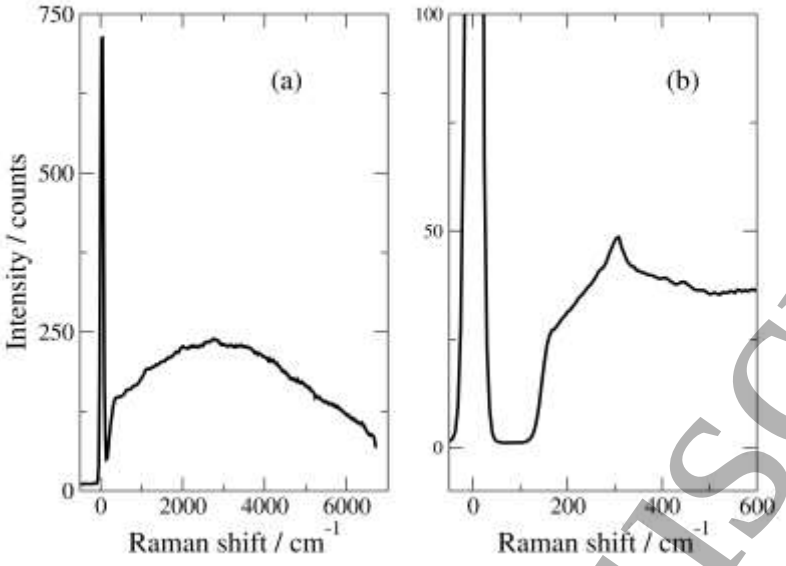

Figure 10. Raman spectra of CdS/λ-DNA nanowires. The excitation light was supplied by a diode laser (λ = 488 nm) focused to the diffraction-limited spot size and the back-scattered light was dispersed on a grating of **(a)** (150 lines mm^{-1} and **(b)** 1800 lines mm^{-1} and then collected on a Peltier-cooled CCD (-60ºC). The spectra shown were obtained by averaging over the spectra of the track deposits in figures 9c and 9d. The Raman edge filter cut-off at <150 cm^{-1} is apparent as the step in (b).

Figures 9a and 9b show Raman spectral images of two printed droplets on glass. Figures 9c and 9d show Raman spectral images of two printed tracks on Pt-on-glass IDEs. The colour scale represents the intensity of fluorescent and scattered light integrated over the spectrum acquired at each pixel. The droplet in figure 9a was printed at a platen temperature of 100ºC and that in figure 9b at 60ºC. Rapid drying of the droplet at the higher temperature results in the precipitation of CdS/λ-DNA in the centre of the 'coffee-ring'. In figures 9c and 9d one 'rail' of a CdS/λ-DNA track is visible running down the left hand edge of the image, not quite in north-south orientation. When the higher resolution grating is employed, the elastically-scattered light makes a relatively larger contribution to the total intensity (figure 9d) and the Pt electrodes are clearly distinguished as bright bands and the glass gaps as dark bands running parallel to the Pt and normal to the CdS/λ-DNA rail. The wetting behaviour of Pt and glass is rather different and the luminescence is most intense from CdS on the Pt, however fluorescence is also visible across the glass gaps. The electrical characterisation of such devices is reported below.

The Raman and luminescence spectra averaged over the track deposits of figure 9c and 9d are shown in figure 10. In figure 10a, the broad feature extending from the elastically scattered

light peak is the photoluminescence from CdS. Neither DNA nor the glass substrate absorbs at the laser wavelength (488 nm) and therefore the images (figures 9a-c) are dominated by the luminescence of the CdS. Using the higher-resolution grating (figure 10b) we can observe directly the LO phonon in the position expected for CdS (near 305 cm^{-1} [49]). As expected for nanoscale particles, the Raman band in figure 10b is broad and has a tail on the higher energy side which is a characteristic of phonon confinement effects. A closer examination of the data in figure 10a shows the presence of "ripples" on the broad PL peak. These features may arise from vibrational modes of CdS/DNA or a Raman cascade in CdS enhanced by resonance effects at the laser wavelength. The Raman cascade is a less likely explanation because the wavenumber difference between peaks does not match literature observations for CdS [50].

3.3 *Electrical Characterisation of printed CdS/λ-DNA nanowires*

Figure 11a shows current-voltage (IV) characterization of an array of separated droplets printed onto interdigitated Pt electrodes (100L). The Pt electrodes are 10 μm thick and the glass gaps are about 9 μm across, therefore each droplet is large enough to span the interdigitated electrodes. Figure 11b is from a similar device, but the droplets are printed so that they overlap to form train tracks (50L), with the tracks running across the interdigitated Pt electrodes in the manner of figures 9c and 9d. AFM data (supporting information) indicates a similar thickness of tracks (60 ± 19 nm) and droplets (58 ± 13), however, the tracks are wider (17 ± 3.1 μm) than droplets (5.0 ± 1.6 μm).

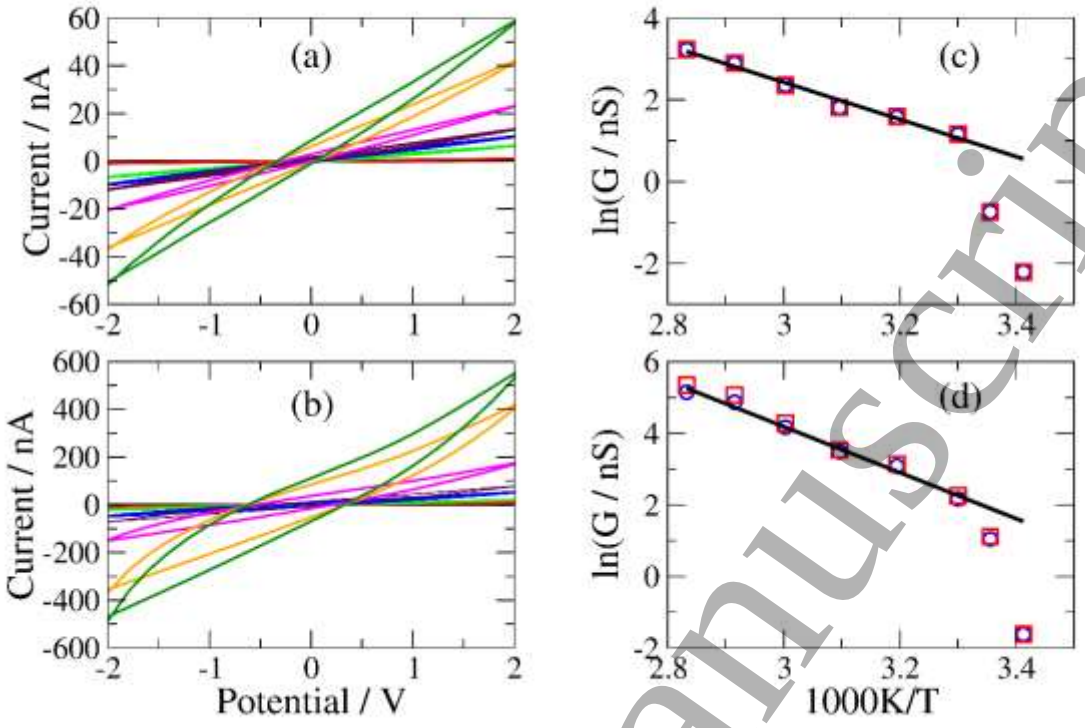

Figure 11. Current-voltage curves for CdS/λ-DNA printed **(a)** droplet 100L and **(b)** track 50L on Pt-on-glass interdigitated electrodes under dry nitrogen atmosphere; (c,d) Arrhenius plots of ln(I) and ln*G* against 1/*T* (c-droplet, d-track). I is the current at +2V bias and G is the differential conductance at zero bias measured for the positive scan in (a) and (b). The temperature range in all the data was 293–353 K.

Although there is some hysteresis in the IV data for both droplets and tracks at the highest temperatures, the curves are approximately linear. At the highest temperatures studied, the conductance for the 50L track devices are about tenfold greater than for the 100L droplet devices, which suggests the track morphology is a much superior method to contact the Pt electrodes, but the track conductance is also more strongly temperature-dependent and the advantage of tracks is less marked near room temperature. After calculating the zero bias conductance *G*, we made an Arrhenius-type plot of ln*G* against 1/*T*. Above about 300 K the plots are quite linear, typical of hopping conductors and the observed activation energies [0.57 ± 0.02 eV (tracks) and 0.39 ± 0.02 eV (droplets)] are notably smaller than simple drop-cast CdS/λ-DNA on the same IDEs [1.03 ± 0.06 eV] [35]. We suggest that this is a result of the extra control achieved in preparing these devices by printing: drop-casting results in a thick film of loosely adherent material whereas printing results in more compact deposits where more intimate nanowire/nanowire contacts are formed. Printing droplets layer-by-layer on a substrate at 60°C also aids in the removal of water from the deposit.

The precise nature of the doping in CdS/λ-DNA nanowires is uncertain, although some information is available from photoluminescence (PL) decay and fluorescence quantum yield measurements of the CdS/λ-DNA nanowire dispersion (supporting information). The data show a rapid initial decay on the sub-nanosecond timescale and a curved semi-logarithmic plot consistent with a broad distribution of decay rates. The steady-state quantum yield is of the order of 1%. These observations are comparable to uncapped CdS nanoparticle data reported previously [51-53], which interprets the luminescence band observed in solution and in the printed deposit (figure 8a) in terms of recombination of trapped electrons/holes. A short PL lifetime and low quantum yield is also consistent with a picture of highly doped CdS as a result of surface defects.

The hysteresis in the current – voltage curves also suggests some ion motion is involved. A simple two-terminal metal/semiconductor/metal device would be expected to show current-voltage characteristics in which the forward and reverse scans retrace. Instead, the presence of mobile ions gives the data a shape more like that for an electrochemical cell or a doped conductive polymer with mobile counterions. Upon application of a bias voltage, the ions accumulate at the electrodes of opposite charge where they form an electrical double layer and the hysteresis is dependent on the rate of this process compared to the potential scan rate. Such coupled electron-ion motion may have a characteristic diffusion-like behaviour, which can be understood on the basis of a transmission line equivalent circuit where separate rails model the electron and ion motion [54]. The data also shows that the hysteresis is more substantial at higher temperature; this suggests that an activated process is involved, but that a simple ion diffusion in adsorbed water is unlikely, because the material is under a dry nitrogen atmosphere and water present will evaporate rapidly at 80^{o}C.

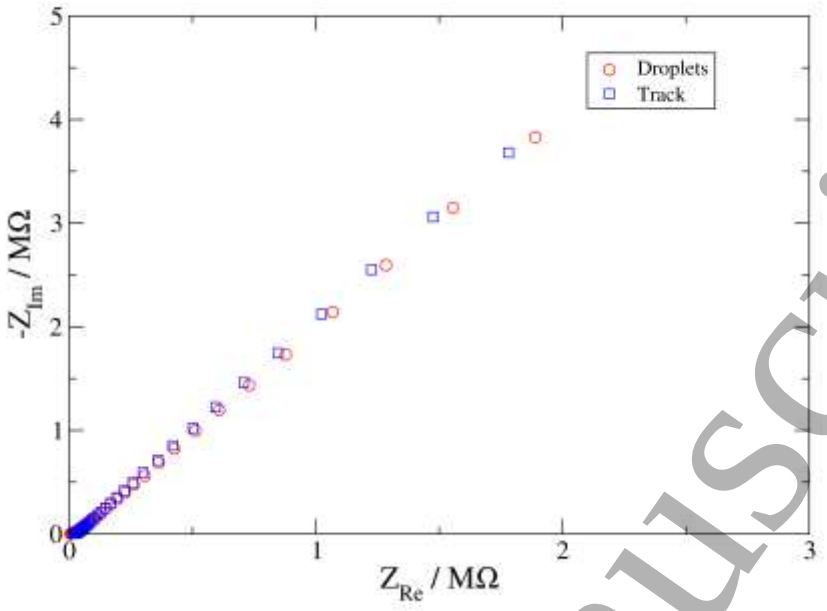

Figure 12. Impedance spectrum (20°C, 10 kHz – 0.16 Hz) for the two-terminal device (CdS/λ-DNA on interdigitated electrodes) of droplet and track printed on Pt interdigitated electrodes.

In figure 12 the impedance spectra for the droplet and the track devices are shown. The frequency-dependence of the impedance (for $f < 1$ Hz) has a power law form $Z_{\mathrm{Re}} = A\omega^{-n}$; $Z_{\mathrm{Im}} = B\omega^{-n}$ with $n = 0.78$ similar to that commonly observed in dielectrics and disordered conductors (Jonscher's law) [55, 56]. This behaviour contrasts with experimental observations on drop-cast CdS/λ-DNA on the same IDEs where we observe a small high frequency semi-circle, suggesting interfacial charge transfer limitations, followed by a Warburg impedance ($n = 0.5$) [35]. $n = 0.5$ is also the expected high frequency behaviour of a transmission line. Detailed interpretation of the mechanism of conduction is not warranted here, but the observed form of the spectrum of figure 12 is typical for hopping in disordered materials [55].

Conclusions

CdS/λ-DNA nanowires were prepared in aqueous dispersion by an established route; they were subsequently formulated as inks simply by addition of ethylene glycol (50% v/v). These inks were successfully printed, using inkjet drop-on-demand technology, as droplet arrays and as tracks by control of the inter-droplet spacing and the substrate temperature. The print head was programmed to make several passes over the arrays in order to deposit multiple layers of material at each point. It was found that printed droplets showed a coffee-ring structure at low

layer numbers <100, but above about 150 layers the additional material occupies the centre of the deposit and a disc is formed. The integrated luminescence intensity from the droplets was proportional to layer number up to 150 layers, after which it became sublinear, which we attribute to inner filter effects. Droplets and tracks were also printed across interdigitated Pt on glass microelectrodes to make simple two-terminal Pt/CdS/λ-DNA/Pt devices. These devices showed approximately ohmic IV behaviour, with some hysteresis as the temperature was increased. The zero-bias conductance showed Arrhenius-like activated behaviour with an activation energy of 0.57 ± 0.02 eV (tracks) and 0.39 ± 0.02 eV (droplets). These values are much less than the CdS band-gap and we attribute them to electron hopping between CdS grains. The impedance spectra for the devices showed behaviour of the Jonscher form often observed for hopping conductors.

Acknowledgements

X-ray photoelectron spectra were obtained at the National EPSRC XPS Users' Service (NEXUS) at Newcastle University, an EPSRC Mid-Range Facility (NS/A000015/1). Financial support is acknowledged from the Bolashak International Scholarship of the President of the Republic of Kazakhstan administered by the JSC "Centre for International Programmes", the Ministry of Education and Science of the Republic of Kazakhstan.

References

[**1**] Houlton A, Pike A R, Galindo M A and Horrocks B R 2009 *Chem. Commun*. 1797–1806
[**2**] Dong L, Hollis T, Connolly B A, Wright N G, Horrocks B R and Houlton A 2007 *Adv. Mater*. **19** 1748–51
[**3**] Su J, Gao F and Hou L 2013 *Mater. Lett*. **92** 206–9
[**4**] Dittmer W U and Simmel F C 2004 *Appl. Phys. Lett*. **85** 633–35
[**5**] Coffer J L, Bigham S R, Pinizzotto R F and Yang H 1992 *Nanotechnology* **3** 69–76
[**6**] Levina L, Sukhovatkin W,. Musikhin S, Cauchi S, Nisman R, Bazett-Jones D P and Sargent E H 2005 *Adv. Mater*. **17** 1854–57
[**7**] Mohamed H D A, Watson S M D, Horrocks B R and Houlton A 2012 *Nanoscale* **4** 5936–45
[**8**] Liu J, Uprety B, Gyawali S, Woolley A T, Myung N V and Harb J N 2013 *Langmuir* **29** 11176–84
[**9**] Sarangi S N, Rath S, Goswami K, Nozaki S and Sahu S N 2010 *Phys. E* **42** 1670–74
[**10**] Braun E, Eichen Y, Sivan U and Ben-Yoseph G 1998 *Nature* **391** 775–78
[**11**] Becerril H A, Stolenberg R M, Wheeler D R, Davis R C, Harb J N and Woolley A T 2005 *J. Am. Chem. Soc.* **127** 2828–29
[**12**] Yan H, Park S H, Finkelstein G, Reif J H and LaBean T H 2003 *Science* **301** 1882–84
[**13**] Keren K, Berman R S and Braun E 2004 *Nano Lett*. **4** 323–26
[**14**] Burley G A, Gierlich J, Mofid M R, Nir H, Tal S, Eichen Y and Carell T 2006 *J. Am. Chem. Soc.* **128** 1398–99

[**15**] Mertig M, Ciacchi L C, Seidel R, Pompe W and De Vita A. 2002 *Nano Lett.* **2** 841–44
[**16**] Monson C F and Woolley A T 2003 *Nano Lett*. **3** 359–63
[**17**] Gu Q and Haynie D T, 2008 Mater. Lett. **62** 3047–50
[**18**] Richter J, Mertig M, Pompe W, Monch I and Schackert H K 2001 Appl. Phys. Lett. **78** 536–38.
[**19**] Mohamed H D A, Watson S M D, Horrocks B R, Houlton A 2015 *J. Mater. Chem. C* **3** 438-46
[**20**] Ma Y, Zhang J, Zhang G and He H 2004 *J. Am. Chem. Soc*. **126** 7097–101
[**21**] Nickels P, Dittmer W U, Beyer S, Kotthaus J P and Simmel F C 2004 *Nanotechnology* **15** 1524–29
[**22**] Dong L, Hollis T, Fishwick S, Connolly B A, Wright N G, Horrocks B R and Houlton A 2007 *Chem. – Eur. J.* **13** 822–28
[**23**] Watson S M D, Hedley J H, Galindo M A, Farha Al-Said S A, Wright N G, Connolly B A, Horrocks B R and Houlton A 2012 *Chem. – Eur. J.* **18** 12008–19
[**24**] Al-Hinai M, Hassanien R, Watson S M D, Wright N G, Houlton A and Horrocks B R 2016 *Nanotechnology* **27** 095704.
[**25**] Watson S M D, Galindo M A, Horrocks B R and Houlton A 2014 *J. Am. Chem. Soc*. **136** 6649–55
[**26**] Bensimon A, Simon A, Chiffaudel A, Croquette V, Heslot F and Bensimon D 1994 *Science* **265** 2096–98
[**27**] Hassanien R, Al-Hinai M, Al-Said S A F, Little R, Šiller L, Wright N G, Houlton A and Horrocks B R 2010 *ACS Nano* **4** 2149–59
[**28**] Watson S M D, Pike A R, Pate J, Houlton A and Horrocks B R 2014 *Nanoscale* **6** 4027–37
[**29**] Westwater J, Gosain D P, Tomiya S, Usui S and Ruda H 1997 *J. Vac. Sci. Technol. B Microelectron. Nanometer Struct.* **15** 554–557
[**30**] Al-Hinai M N, Hassanien R, Wright N G, Horsfall A B, Houlton A and Horrocks B R 2013 *Faraday Discuss*. **164** 71–91
[**31**] Finn D J, Lotya M and Coleman J N 2015 ACS *Appl. Mater. Interfaces* **7** 9254−9261
[**32**] Dang M C, Dang T M D and Fribourg-Blanc E 2013 *Adv. Nat. Sci*: *Nanosci. Nanotechnol.* **4** 015009
[**33**] Calvert P 2001 *Chem. Mater.* **13** 3299-3305
[**34**] Jang D, Kim D and Moon J 2009 *Langmuir* **25** 2629–2635
[**35**] Nurdillayeva R N, Horrocks B R and Pike A R 2017 *Materials Today: Proceedings INESS 2017* in press
[36] Fenneman D B 1982 *J. Appl. Phys.* **53** 8961–8968
[37] Zahn M, Ohki Y, Fenneman D B, Gripshover R J and Gehman Jr. V H 1986 *Proc. IEEE* **74** 1182–1221
[**38**] Watson S M D, Houlton A and Horrocks B R 2012 *Nanotechnology* **23** 505603
[**39**] Lee H-H, Chou K-S and Huang K-C 2005 *Nanotechnology.* **16** 2436–2441
[**40**] Cui W, Lu W, Zhang Y, Lin G, Wei T and Long Jiang L 2010 *Colloids and Surfaces A: Physicochem. Eng. Aspects* **358** 35–41
[**41**] Lee C-L, Chang K-C and Syu C-M 2011 *Colloids and Surfaces A: Physicochem. Eng. Aspects* **381** 85–91
[**42**] Costa C, Pinheiro C, Henriques I and Laia C A T 2012 *ACS Appl. Mater. Interfaces* **4** 1330−1340
[**43**] Finn D J, Lotya M and Coleman J N 2015 ACS *Appl. Mater. Interfaces* **7** 9254−9261
[**44**] Gaiardo A, Fabbri B, Guidi V, Bellutti P, Giberti A, Gherardi S, Vanzetti L, Malagù C and Zonta G 2016 *Sensors 16* 296−314

[**45**] Zhu L, Feng C, Li F, Zhang D, Li C, Wang Y, Lin Y, Ruan S and Chen Z 2014 *RSC Adv*. **4** 61691–61697
[**46**] Deegan R D, Bakajin O, Dupont T F, Huber G, Nagel S R and Witten T A 1997 *Nature* **389** 827–829
[**47**] Hu H and Larson R G 2006 *J. Phys. Chem. B* **110** 7090–7094
[**48**] Ooi Y, Hanasaki I, Mizumura D and Matsuda Y 2017 *Science and Technology of Advanced Materials* **18** 316–324
[**49**] Nusimovici M A and Birman J L 1967 *Phys. Rev.* **156** 925–938
[**50**] Leite R C C, Scott J F and Damen T C. 1969 *Phys. Rev. Lett.* **22** 780–782
[**51**] Chestnoy N, Harris T D, Hull R and Brus L E 1986 *J. Phys. Chem.* **90** 3393–3399
[**52**] O'Neil M, Marohn J and McLendon G 1990 *J. Phys. Chem.* **94** 4356–4363
[**53**] Veamatahau A, Jiang B, Seifert T, Makuta S, Latham K, Kanehara M, Teranishi T and Tachibana Y 2015 *Phys. Chem. Chem. Phys.* **17** 2850-2858
[**54**] Albery W J, Chen Z, Horrocks B R, Mount A R, Wilson P J, Bloor D, Monkman A T and Elliott C M 1989 *Faraday Discuss*. **88** 247-259
[**55**] Jonscher A K 1977 *Nature* **256** 673–679
[**56**] Jonscher A K 1981 *J. Mater. Sci*. 16 2037–2060